International Journal of Multidisciplinary Research and Publications
ISSN (Online): 2581-6187

The Dolerites of the Léré Region (Southwestern Chad, Africa): Petrography and Geochemical Characterisation

Jean-Claude Doumnang Mbaigané[1], Léontine Tekoum[1], Pierre Rochette[2], Jean-Paul Vicat[1*]
[1]Laboratory of Geology, Geomorphology, and Remote Sensing, Faculty of Exact and Applied Sciences, University of N'Djamena, P.O. box 1027, N'Djamena, Republic of Chad
[2]Aix-Marseille University, CNRS, IRD, INRAE, CEREGE BP 80, 13545, Aix-en-Provence, France
Email address: jpvicat@gmail.com

Abstract– *The dolerites of the Léré region were emplaced within Pan-African faults reactivated during the formation of the Cretaceous basin, between the Neocomian and the Eocene. They exhibit varied textures, including intergranular, ophitic, and subophitic. Based on mineralogical composition, two groups are distinguished: one primarily composed of andesine, labradorite, clinopyroxene, orthopyroxene, and titanomagnetite, and the other mainly of andesine, labradorite, clinopyroxene, amphibole, and biotite. The dolerites of the Léré basin are classified as basalt and trachybasalt. Contamination by the continental crust during their emplacement is minimal. Their varied chemical compositions correlate with their geographical positions. Dolerites with tholeiitic or transitional compositions are located in the Proterozoic basement, while initial rifting tholeiites are found only in the Cretaceous basin. Alkaline dolerites are rare in both the Proterozoic basement and the Cretaceous basin. This distinction in chemical composition and geographical location is evident in analyses of the Mayo Oulo-Léré basin available in the literature. Mantle sources, located at various depths, have compositions between those of OIB and E-MORB. The magmas that originated the dolerites of the Léré basin come from different sources at different depths. Alkaline basalts originate from the garnet zone, continental tholeiites from the spinel zone, and other dolerites from the garnet-spinel transition zone. The degrees of partial melting are approximately 2–3% for magmas producing the alkaline and transitional basalts, and 5–10% for those producing the tholeiites.. Continental tholeiites and transitional basalts have a mixed asthenospheric-lithospheric source. Initial rifting tholeiites and alkaline dolerites have an asthenospheric mantle source attributed to crustal thinning in the Léré basin. The IRT dolerites signature is consistent with the Cretaceous Mayo-Oulo Léré basin belonging to the West African and Central Rift System.*

Keywords– *Chad, Cretaceous Léré basin, dolerites, Proterozoic basement.*

I. Introduction

In southwestern Chad, the Léré region exposes a Neoproterozoic basement intersected by the Cretaceous Léré basin. The Léré basin is the extension into Chad of the Cameroonian Mayo Oulo basin. The Mayo Oulo-Léré basin, along with the Babouri-Figuil and Hama-Koussou Cretaceous basins, are small basins located to the northeast of the Yola-Guéra basin, which forms the eastern termination of the Benue Trough (Fig. 1).

Other small Cretaceous basins, including Koum, Vina, Babouan, Djérem, and Mberé, are known in Cameroon, south of the Yola-Guéra Basin. In Chad, the small Cretaceous basins of Pala and Lamé constitute the western termination of the Bongor and Doba basins masked by Quaternary cover (Fig. 1). The Benue Trough and the small Cretaceous basins of Cameroon and Chad are part of the larger West and Central African Rift System (WCARS), which extends from the Benue to Sudan (Fig. 1). The formation of WCARS is linked to the separation of the Southern Atlantic Ocean [1–3].

Dykes of magmatic rocks, predominantly doleritic, intersect the Mayo Oulo-Léré, Babouri-Figuil, and Hama-Koussou basins, as well as the Proterozoic basement, along a major fracture system trending approximately N-S, NE-SW, and E-W. These dolerites are attributed to magmatism with varied chemical affinities, both tholeiitic and alkaline [4–10].

The magmatism of the Léré Basin has been much less studied than that of the Cameroonian basins. This study provides new geochemical data (major and trace elements) on the Léré dolerites and aims to characterize their nature, petrogenetic processes, origin, and geotectonic context.

II. Geological Setting

The Léré region is part of the Chadian Mayo-Kebbi Massif. This region has been the subject of numerous studies [5, 11–17]. The Mayo-Kebbi Massif consists of a basement of Proterozoic metamorphic and magmatic rocks overlain with Cretaceous and more recent formations. The basement region is part of the Pan-African Central African Fold Belt [18] resulting from the collision, around 600 Ma, between the Congo and West African cratons [19–20]. In the studied area (Fig. 2), the Neoproterozoic basement consists of the epi to mesozonal metamorphic belt of Zalbi and granitoid batholiths. The Zalbi metamorphic belt, trending SSW–NNE, comprises from bottom to top meta- ultrabasites, meta-basalts, meta-gabbros, and meta-pyroxenites interbedded with chlorite schist, followed by meta-epiclastites, quartz-rich sericite schists, silty and sandy claystones, and finally black shales overlain by a stack of spilitic flows [16]. The Zalbi belt is affected by an isoclinal folding striking NNE-SSW with axial planes dipping to the west and the development of schistosity [5]. The Zalbi trough is intruded by calc-alkaline gabbro and diorites dated by Pb/Pb to 737 Ma [15] related to an active margin setting [16]. Regionally, a second intrusion phase of tonalites is dated by Pb/Pb from 664 to 638 Ma [15]. The previous formations are

Jean-Claude Doumnang Mbaigané, Léontine Tekoum, Pierre Rochette, and Jean-Paul Vicat, "The Dolerites of the Léré Region (Southwestern Chad, Africa): Petrography and Geochemical Characterisation," *International Journal of Multidisciplinary Research and Publications (IJMRAP)*, Volume 7, Issue 10, pp. 22-32, 2025.

intruded by post-orogenic calc-alkaline granitoids dated by Pb/Pb at 570 Ma [15]. The Léré region is interpreted as a volcanic arc formed by the eastward subduction of an oceanic domain [20, 21]. According to this interpretation, the Zalbi tectonic belt represents the suture zone of the former Pan-African ocean.

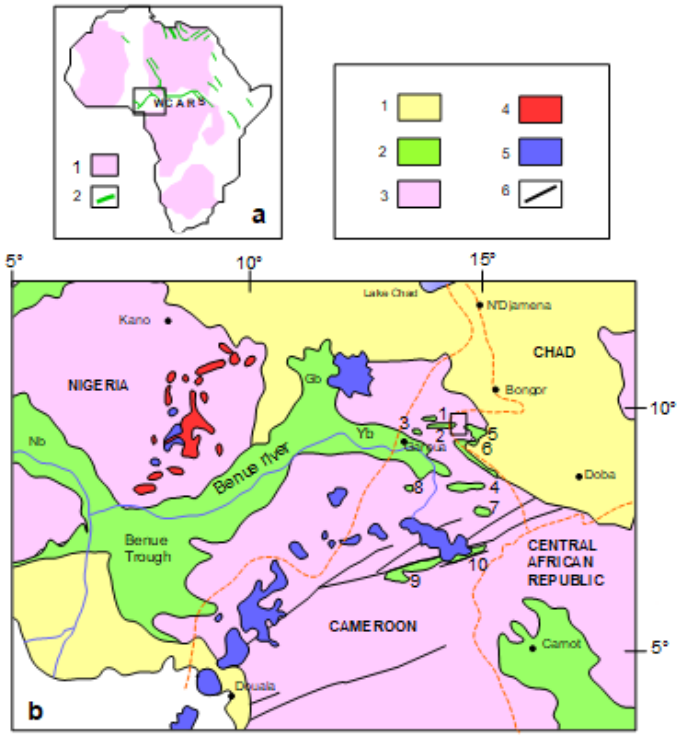

Fig. 1. (a) Distribution of cratons and Mesozoic rifts in Africa. 1: Cratons. 2: Mesozoic rifts. WCARS: West and Central African rifts system. Inset: Location of Fig. b. (b) Geological sketch map of the Benue Trough. 1: Quaternary sediments. 2: Cretaceous to Tertiary sediments. 3: Crystalline basement. 4: Jurassic ring complexes. 5: Cenozoic to recent magmatism of the Cameroon Line. Nb: Niger branch. Yb: Yola branch. Gb: Gongola branch. Cretaceous basins of Northern Cameroon and Chad: 1, Babouri-Figuil; 2, Mayo Oulo (Cameroon)–Léré (Chad); 3, Hama-Koussou; 4, Koum; 5, Pala; 6, Lamé; 7, Vina; 8, Babouan; 9, Djérem; 10, Mberé. Inset: location of Fig. 2.

The Mayo Oulo-Léré Basin is an asymmetrical synclinal system trending N110°E, extending over 50 km with a maximum width of 10 km. The thickness of the deposits is about 2.5 km [22]. The asymmetry of the structure is due to major normal faults along the southern edge of the basin, which formed during its progressive infilling [23, 24]. The basin comprises conglomerates and coarse sandstones at the base, overlain by a thick series of alternating sandstones, marlstones, shales, and carbonates [25, 26]. Near the base of the series, pillow basalts are interbedded within the shales [27]. The sediments were deposited in a fluviolacustrine environment [22] under varied climatic conditions, fluctuating from more humid at the bottom to more arid at the top [28]. In the Mayo Oulo Basin, fossils found in the middle part of the series indicate a Barremian sedimentation [27]. Sedimentation is older for the lower levels [27] and more precisely towards the Valanginian–Hauterivian transition [29]. In the upper levels of the series, the presence of Monoporate pollen (*Monoporopollenites annulatus*) is indicative of a Tertiary age (Eocene or younger) [22].

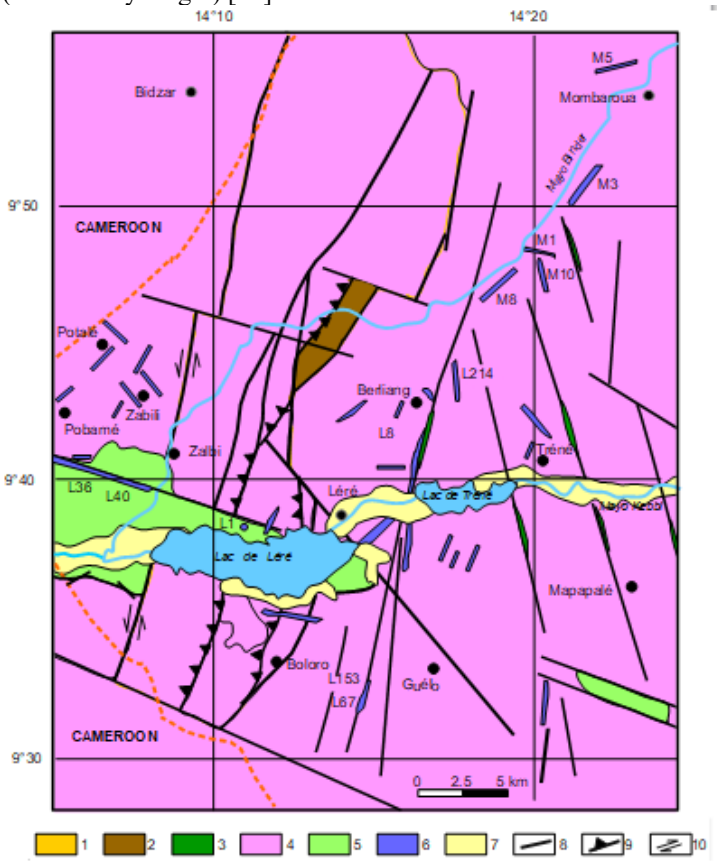

Fig. 2. Geological sketch map of the studied area, modified after [5, 16]. 1: Zalbi series (undifferentiated meta-mafic rocks, meta-sediments, and spilites). 2: Meta-gabbros and diorites intruding the Zalbi series. 3: Amphibolites. 4: Pan-African post-orogenic granitoids. 5: Cretaceous sedimentary rocks. 6: Dolerites. 7: Alluvium. 8: Fault. 9: Reverse fault. 10: Strike-slip motion. The analysed samples are referenced.

Most of the deformation observed in the Mayo Oulo-Léré basin, as in the Babouri-Figuil and Hama Koussou basins, are synsedimentary. The post-sedimentary deformations, such as reverse faults, bed-to-bed sliding, and strike-slip faults [23] are minor and indicate an N-S shortening direction. This tectonic event is related to the late Cretaceous tectonic phase as defined in the Benue Trough [30] and also to the late Eocene compression [31, 32].

The Léré region is intruded by dolerite dykes following several directions: N0° to N15°E, N40°E to N65°E, and N100°E to N160°E. These dykes vary in thickness from a few meters to about fifty meters and in length from hundreds of meters to several tens of kilometers. These dykes are related to the rejuvenation of Precambrian faults [4, 23]. The dykes that intersect the Cretaceous basins develop a local contact metamorphism [29]. Structural field data indicate that the doleritic dykes are older than the regional compressive event of the Late Eocene [31, 32].

There is no radiometric dating of the basic magmatism in the Mayo Oulo-Léré basin. However, in northern Cameroon and southwestern Chad, basaltic dykes have K-Ar ages ranging between 43 and 87 Ma [33]. In Chad, near the Léré Basin, a

Jean-Claude Doumnang Mbaigané, Léontine Tekoum, Pierre Rochette, and Jean-Paul Vicat, "The Dolerites of the Léré Region (Southwestern Chad, Africa): Petrography and Geochemical Characterisation," *International Journal of Multidisciplinary Research and Publications (IJMRAP)*, Volume 7, Issue 10, pp. 22-32, 2025.

dolerite sill drilled in the Bongor Basin has been dated at 52–56 Ma, and basaltic sills of 97–101 Ma have been found west of Doba, in the Doseo Basin [34]. These ages are compatible with the functioning of the Mayo Oulo-Léré basin from the Neocomian to the Eocene.

The dykes that crosscut the Proterozoic basement might be, in part, older, as pre-Mesozoic basic intrusions are known further South in Cameroon, in the Garoua region [35] and further East in Chad, in the Doba basin [36] and the Guéra massif [37].

III. Samples and Analytical Methods

Forty-five samples of basic dykes from the Léré region were collected during field works conducted in Mayo Kebbi West. Thin sections and mineral analyses were performed at Orléans University (France) using a CAMECA Microbeam apparatus. The following technical parameters were used: accelerating voltage of 15 kV, beam current of 10 to 20 nA, and a counting time of 10 seconds. Standards used were a combination of natural and synthetic minerals.

Rocks analyses were conducted at the CRPG (Petrographic and Geochemical Research Center) in Nancy, France. Major and trace element concentrations were measured using ICP-OES and ICP-MS, respectively. The samples were ground to 70 µm, and approximately 300 mg of powder was prepared by alkaline fusion with $LiBO_2$ at 1000°C and dissolved in 1N HNO_3. Calibration and quality control were conducted using international geostandards [38].

IV. Results

4.1 Field occurrence

The dolerite dyke outcrop in three directions: N110°E, near NE-SW (N40°E to N75°E), and near N-S (N0°, N10°E, N165°E). They are sub-vertical and appear as continuous outcrops or aligned dark green boulders with a thin brown patina.

A dyke trending N110°E crosscuts the Cretaceous sediments of the Léré Basin on its northern edge. This subvertical dyke is several kilometers long and ranges from one to a hundred meters in thickness. It is associated with sills interlayered in the sandstone sediments of the basin. This N110°E dyke extends westward into Cameroon along the northern edge of the Mayo Oulo Basin. Its total length is approximately 20 km. Two small dykes approximately N110°E, one south of Pobamé and the other south of Léré Lake, crosscut the Proterozoic basement.

The dykes near N-S and NE-SW, ranging from one to ten meters in thickness and one to three kilometers in length, crosscut the Proterozoic basement. The N-S dykes exhibit vacuoles resulting from plagioclase dissolution and a mineral fabric following their direction.

At Dissing, a circular intrusion, about forty meters in diameter, outcrops in the Cretaceous basin near its northern edge. The core, likely more mafic, has undergone intense alteration, leaving a hollow in the massif, which outcrops as a circular shape more or less masked by sandy deposits.

4.2 Petrography

In hand specimens, feldspars are easily visible to the naked eye as automorphic phenocrysts (2-10 mm) and numerous whitish microcrystals (<2 mm) that stand out in a dark green matrix of oxides, pyroxenes, and amphiboles. Based on their mineralogical composition, under the polarized microscope, the dolerites are divided into two groups: orthopyroxene and clinopyroxene dolerites (D2P) and clinopyroxene-only dolerites (D1P).

The D2P dolerites are found in the N110°E dyke on the northern edge of the Léré Cretaceous basin. These dolerites display sub-ophitic to ophitic textures. They contain plagioclases, clinopyroxenes, orthopyroxenes, opaque minerals, and occasionally rare alkali feldspar phenocrysts. The mesostase consists of plagioclase microlites and titanomagnetite. Accessory minerals include epidote and chlorite. The plagioclase appears as large laths and interstitial microlites. These plagioclases (An 35-62%) are either andesine or labradorite. Occasionally, some interstitial alkali feldspars are present. Orthopyroxenes in the form of large intergranular crystals are hypersthene (Mg%: 61–66; Ca%: 3–4; Fet + Mn%: 29–34). Clinopyroxenes appear as large prismatic crystals between the plagioclase laths, identified as calcium-rich augites (Mg%: 35–43; Ca%: 38–42; Fet + Mn%: 23–34). The opaque minerals are generally titanomagnetite (TiO_2=20.4%), occurring as millimeter-sized automorphic to subautomorphic crystals between the plagioclase laths or included in the pyroxenes. The D2P dolerites sometimes contain quartz xenocrysts.

The D1P dolerites include the dykes that crosscut the Pan-African basement and the Dissing pluton that intrudes the Cretaceous basin. The dykes that intersect the Pan-African basement exhibit various textures, including intergranular, ophitic, and sub-ophitic. They contain plagioclases, clinopyroxenes, amphiboles, black micas, opaque minerals, and occasionally rare alkali feldspars. The mesostase is composed of plagioclase microlites and titanomagnetite. Accessory minerals include epidote, chlorite, and occasionally titanite and sulfides. Plagioclase in laths and microlites are andesine and labradorite (An-37-64). Sometimes, interstitial alkali feldspars are present. Clinopyroxenes, in large automorphic crystals, have varied compositions. They include diopside (Ca%: 46–47; Mg%: 36–40; Fet+Mn%: 14–17), hedenbergite (Ca%: 46–47; Mg%: 25–27, Fet+Mn%: 26–28), and calcium-rich augite (Ca%: 31–43; Mg%: 36–37, Fet+Mn%: 20–33). Diopside appears more frequently in the N0°E dykes, while augite and hedenbergite are found mainly in the N45°E to N100°E dykes. The amphiboles are actinolite or magnesiohornblende. Black micas, often abundant in the N0°E dykes, are either biotite (XFe=0.54) or phlogopite (XFe=0.34). Titanomagnetites, in millimeter-sized microphenocrysts, crystallize between the plagioclase laths and pyroxene crystals. In the most altered facies, opaque minerals resulting from the destabilization of pyroxenes and millimeter-sized carbonate ocelli (2 to 3% by volume) are observed. The D1P dolerites often contain quartz and alkali feldspar xenocrysts, as well as xenoliths of granitoid from the Pan-African basement.

The Dissing pluton consists of dolerite with intersertal to sub-ophitic texture. The abundant plagioclases, in laths and

Jean-Claude Doumnang Mbaigané, Léontine Tekoum, Pierre Rochette, and Jean-Paul Vicat, "The Dolerites of the Léré Region (Southwestern Chad, Africa): Petrography and Geochemical Characterisation," *International Journal of Multidisciplinary Research and Publications (IJMRAP)*, Volume 7, Issue 10, pp. 22-32, 2025.

microlites, are accompanied by alkali feldspars. Clinopyroxene phenocrysts are augites, and the millimeter-sized amphiboles are hornblendes. Biotite, titanomagnetite, and sometimes apatite are also present. The feldspars are often altered to chlorite, epidote, or calcite.

4.3 Geochemistry

Geochemical compositions of Léré dolerites are reported in Table 1.

The samples exhibit a relatively heterogeneous chemical composition, with the following ranges: SiO_2 (45.05–49.34 wt%), TiO_2 (1.08–3.44 wt%), Al_2O_3 (14.54–16.17 wt%), Fe_2O_3 (11.05–16.91 wt%), MgO (4.01–6.79 wt%), Na_2O+K_2O (3.61–4.97 wt%), CaO (6.25–10.32 wt%), and P_2O_5 (0.24–0.62 wt%). The Mg# number (100MgO/40.32)/((MgO/40.32) + (FeO/71.85)) evolves from 35.84 to 55.98.

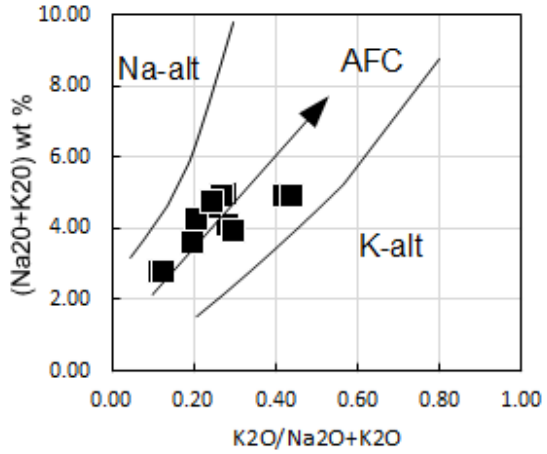

Fig. 3. Plot of Léré dolerites in Na_2O+K_2O vs K_2O / (K_2O + Na_2O) diagram from [40]. AFC: Assimilation and fractional crystallization. Na-alt, K-alt: Na and K alteration.

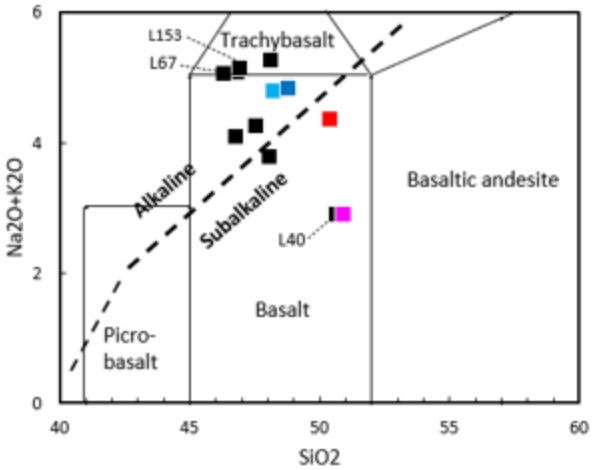

Fig. 4. Total Alkali-Silica diagram from [42] (wt% volatile-free recalculated compositions). The dotted line represents the boundary between the tholeiitic and alkaline fields after [43]. Symbols: pale blue, L8; dark blue, L1; red, M8; magenta, L36; black, other dolerites.

The sometimes high LOI values (1.14–5.4%) can indicate a notable degree of alteration. However, in the diagram from [40] (Fig. 3), Léré dolerites plot outside the field of Na-K alteration, showing that the analysed samples are not significantly altered. Moreover, the Y/Ho ratios (25.4–29.9), similar to those of unaltered basalts (mean value 28) after [41], confirm the absence of significant alteration in the Léré dolerites.

In the Total Alkali-Silica diagram from [42] (Fig. 4), four samples (L153, L214, L67, M3) can be classified as trachybasalts and eight as basalts. Most basalts plot above or near the subalkaline-alkaline boundaries defined by [43], while two samples (L36 and L40) clearly plot in the subalkaline domain.

The petrographic study showed that the Léré dolerites are more or less altered, with the formation of secondary minerals. As a result, the concentrations of Na and K, which are very mobile elements, may have been modified even in the absence of significant alteration.

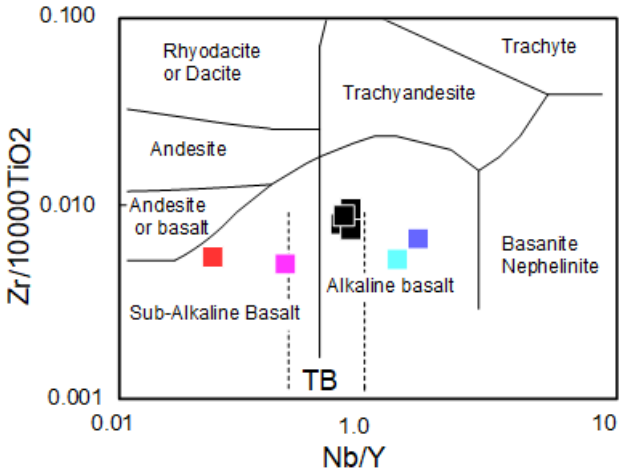

Fig. 5. Plot of Léré dolerites in the diagram Zr/Ti vs Nb/Y from [44], except samples L153, L67 and L40 for which trace elements are not available. The dotted black lines limit the domain of the transitional basalts (TB) after [45]. Symbols as in Fig. 4.

For the samples with available trace element data, the Zr/Ti vs. Nb/Y diagram [44] (Fig. 5), based on immobile elements, shows that two samples (M8, L36) have a sub-alkaline basalt composition, while the other dolerites exhibit an alkaline basalt composition. According to [45], L8 and L1 are distinctly alkaline (Y/Nb < 1), while the other alkaline samples are more transitional (1< Y/Nb < 2).

Except for M8, the subalkaline dolerites (L40 and L36) contain normative quartz. In contrast, the alkaline dolerites (L8 and L1) contain normative nepheline, and the transitional samples contain neither quartz nor nepheline (Table 1).

To differentiate subalkaline dolerites the FeO/MgO vs SiO_2 diagram from [46] is preferred over the AFM diagram from [43] due to the mobility of Na and K. In this diagram (not shown here), the subalkaline samples (L40, L36) plot within the tholeiitic field.

Jean-Claude Doumnang Mbaigané, Léontine Tekoum, Pierre Rochette, and Jean-Paul Vicat, "The Dolerites of the Léré Region (Southwestern Chad, Africa): Petrography and Geochemical Characterisation," *International Journal of Multidisciplinary Research and Publications (IJMRAP)*, Volume 7, Issue 10, pp. 22-32, 2025.

TABLE 1. Major and trace element analyses of Léré dolerites. CIPW normative compositions and Mg#=molar ratio of [100*MgO / (MgO + FeO)] calculated according to $Fe_2O_3/FeO=0.15$. $Eu/Eu^*=Eu_N / (Sm_N \times Gd_N)^{1/2}$ where N indicates that the values are normalized to the C1 chondrite of [39]. $Ba/Ba^*=Ba_N / (Rb_N \times Th_N)^{1/2}$, $Nb/Nb^*=Nb_N / (K_N \times La_N)^{1/2}$, $Ta/Ta^*=Ta_N / (K_N \times La_N)^{1/2}$, $Ti/Ti^*=Ti_N / (Eu_N \times Dy_N)^{1/2}$, and $Sr/Sr^*=Sr_N / (Ce_N \times P_N)^{1/2}$, where N indicates that the values are normalized to the primordial mantle [39]. D1P: clinopyroxene dolerite. D2P: clinopyroxene and orthopyroxene dolerite. Trace element ratios quoted in the text are calculated.

Sample	L153	L214	M10	L67	M3	M1	M5	L8	L1	M8	L40	L36
Rock type	**D1P**	**D1P**	**D1P**	**D1P**	**D1P**	**D1P**	**D1P**	**D1P**	**D1P**	**D1P**	**D2P**	**D2P**
SiO2 (Wt %)	45.72	45.58	45.97	45.54	45.41	46.20	45.05	46.28	48.33	49.34	49.01	49.21
TiO2	3.44	3.40	2.50	3.44	2.52	2.90	2.50	2.71	2.64	1.08	1.81	1.80
Al2O3	14.95	15.95	15.56	14.95	15.37	14.97	15.03	14.95	14.54	16.17	14.89	14.78
Fe2O3	16.11	16.14	13.83	16.91	13.98	14.46	14.26	12.57	12.08	11.05	11.10	11.15
MnO	0.18	0.18	0.23	0.20	0.21	0.21	0.28	0.18	0.16	0.31	0.15	0.13
MgO	4.48	4.01	5.82	4.46	4.55	5.16	6.64	4.68	6.79	5.24	6.28	6.25
CaO	7.21	6.25	8.06	7.16	6.81	8.02	8.19	9.60	9.13	10.11	10.32	10.25
Na2O	2.86	3.59	2.93	2.79	3.62	2.90	2.76	3.48	3.61	3.37	2.47	2.44
K2O	2.08	1.38	1.16	2.16	1.32	0.71	1.16	1.10	1.15	0.88	0.32	0.34
P2O5	0.57	0.55	0.48	0.62	0.50	0.50	0.37	0.35	0.54	0.25	0.25	0.24
LOI	2.36	2.91	2.41	2.36	5.40	3.80	3.39	3.88	1.14	1.60	3.23	3.25
Total	99.96	99.94	99.07	99.96	99.80	99.97	99.73	99.89	100.10	99.45	99.92	99.84
Quartz											1.6	1.9
Orthose	12.8	8.5	7.2	13.2	8.4	4.4	7.2	6.9	6.9	5.4	2.0	2.1
Albite	25.2	31.8	26.0	24.4	32.9	25.9	24.6	27.1	29.5	29.4	21.9	21.6
Anorthite	22.7	24.4	27.1	22.6	23.4	27.2	26.5	23.1	20.5	27.3	29.9	29.7
Néphéline								2.2	0.9			
Diopside	9.2	3.9	9.8	8.7	8.1	9.8	11.5	20.7	18.4	19.1	18.1	18.1
Hypersthène	4.7	4.6	7.5	4.1	0.4	18.6	3.4			2.8	20.4	20.5
Olivine	14.4	15.8	13.7	15.8	17.8	4.6	18.3	11.5	15.2	11.4		
Magnétite	2.9	2.9	2.5	3.0	2.6	2.6	2.6	2.3	2.1	2.0	2.0	2.0
Ilménite	6.8	6.8	5.0	6.8	5.1	5.8	5.0	5.4	5.1	2.1	3.6	3.6
Apatite	1.3	1.3	1.1	1.4	1.2	1.2	0.9	0.8	1.2	0.6	0.6	0.5
TOTAL	100.0	100.0	100.0	100.0	100.0	100.0	100.0	100.0	100.0	100.0	100.0	100.0
mg#	38	36	49	37	42	45	51	46	56	52	56	56
Ba (ppm)			507	767	469	596	430	286	483	160		82
Cr			70	26	20	30	130	40	295	280		243
Cs			0.55	1.18	2.11	0.22	1.90	0.27	0.45	0.28		<0.02
Ga			22.60	24.50	23.50	23.80	21.90	22.80	18.32	16.60		19.83
Hf			4.70	7.14	6.20	6.90	4.90	3.60	4.32	1.80		2.30
Nb			22.00	29.81	25.50	31.30	21.50	26.90	35.48	4.50		8.47
Rb			20.60	41.73	27.20	14.90	23.20	18.90	18.90	13.10		6.91
Sn			2.00	3.25	2.00	2.00	2.00	2.00	1.00	1.00		1.59
Sr			664	510	569	818	581	700	725	236		289
Ta			1.50	2.26	1.60	2.00	1.50	1.60	2.15	0.30		0.60
Th			1.92	2.73	2.96	2.85	1.97	1.96	2.78	1.11		0.81
Tl			<0.5	<0.5	<0.5	<0.5	<0.5	<0.5	<0.5	<0.5		<0.5
U			0.56	0.70	0.64	0.64	0.57	0.57	0.88	0.35		0.26
V			255	258	187	286	274	340	219	275		197
W			1.00	0.73	1.00	1.00	1.00	<1	<1	1.00		0.29
Y			25.00	36.26	28.90	36.70	24.60	20.10	21.51	18.70		17.92
Zr			190	299	250	280	190	140	182	60		89
La			23.90	39.59	29.00	36.80	24.80	16.10	24.21	9.30		7.04
Ce			54.20	90.09	65.90	81.10	55.50	33.40	49.00	21.10		16.30
Pr			7.06	11.84	8.54	10.50	7.20	4.24	6.06	2.95		2.31
Nd			29.50	49.65	35.90	43.40	29.70	18.40	26.39	13.20		10.50
Sm			6.54	9.77	8.06	9.31	6.59	4.67	6.22	3.51		3.32
Eu			2.20	3.00	2.38	2.66	2.04	1.69	2.22	1.14		1.27
Gd			6.55	9.16	7.72	9.08	6.34	5.20	6.10	3.84		3.77
Tb			0.90	1.29	1.06	1.29	0.90	0.73	0.89	0.55		0.60
Dy			5.08	7.16	6.02	7.25	5.17	4.21	4.75	3.40		3.17
Ho			0.95	1.27	1.12	1.35	0.97	0.78	0.84	0.70		0.60
Er			2.70	3.08	3.01	3.79	2.64	2.14	2.07	2.13		1.61
Tm			0.33	0.40	0.37	0.50	0.35	0.27	0.29	0.28		0.22
Yb			2.18	2.79	2.50	3.13	2.14	1.59	1.55	1.87		1.53
Lu			0.31	0.46	0.34	0.44	0.31	0.24	0.21	0.28		0.20
S REE			142.40	229.55	171.92	210.60	144.65	93.66	130.62	64.25		52.44
Ratios												
LaN/YbN			7.86	10.18	8.32	8.43	8.31	7.26	11.19	3.57		3.30
Eu/Eu*			2.14	3.09	2.58	3.01	2.11	1.61	2.01	1.20		1.16
Y/Ho			26.32	28.55	25.80	27.19	25.36	25.77	25.76	26.71		29.87
Y/Nb			1.14	1.22	1.13	1.17	1.14	0.75	0.61	4.16		2.12
Ba/Ba*			2.68	2.39	1.74	3.04	2.11	1.56	2.22	1.39		1.16
Nb/Nb*			0.84	0.65	0.83	1.24	0.81	1.29	1.37	0.32		1.13
Ta/Ta*			1.00	0.86	0.91	1.37	0.98	1.33	1.44	0.37		1.59

Jean-Claude Doumnang Mbaigané, Léontine Tekoum, Pierre Rochette, and Jean-Paul Vicat, "The Dolerites of the Léré Region (Southwestern Chad, Africa): Petrography and Geochemical Characterisation," *International Journal of Multidisciplinary Research and Publications (IJMRAP)*, Volume 7, Issue 10, pp. 22-32, 2025.

TABLE 1 (continued)

Sample	L153	L214	M10	L67	M3	M1	M5	L8	L1	M8	L40	L36
Rock type	D1P	D1P	D1P	D1P	D1P	D1P	D1P	D1P	D1P	D1P	D2P	D2P
Sr/Sr*			1.21	0.64	0.92	1.20	1.19	1.92	1.30	0.95		1.36
Ti/Ti*			1.21	1.20	1.08	1.07	1.25	1.65	1.32	0.89		1.46
Nb/U			39.29	42.59	39.84	48.91	37.72	47.19	40.54	12.86		32.58
Ba/Nb			23.05	25.72	18.39	19.04	20.00	10.63	13.62	35.44		9.74
La/Nb			1.09	1.33	1.14	1.18	1.15	0.60	0.68	2.07		0.83
Th/Tb			2.13	2.12	2.79	2.21	2.19	2.68	3.12	2.02		1.35
Ta/Tb			1.67	1.75	1.51	1.55	1.67	2.19	2.42	0.55		1.00
La/Sm			3.65	4.05	3.60	3.95	3.76	3.45	3.90	2.65		2.12

The Léré dolerites exhibit variable total REE contents: 52.44–64.25 ppm for tholeiitic dolerites, 93.66–130.62 ppm for alkaline dolerites, and higher values for transitional dolerites (142.40–229.57 ppm). The chondrite-normalized diagrams, (Fig. 6), are characterized by variable fractionation of light rare earth elements compared to heavy rare earth elements. Fractionation is significant for transitional $(La/Yb)_N$=7.86–10.18) and alkaline dolerites (7.26–11.19) but lower for tholeiitic dolerites (3.30–3.57). The transitional dolerites have patterns similar to Ocean Island Basalts (OIB). The europium anomalies, Eu/Eu*, of the tholeiitic dykes (1.16–1.2) are slight. The alkaline and transitional dykes have higher europium anomalies (1.6–2.0 and 2.1–3.1, respectively).

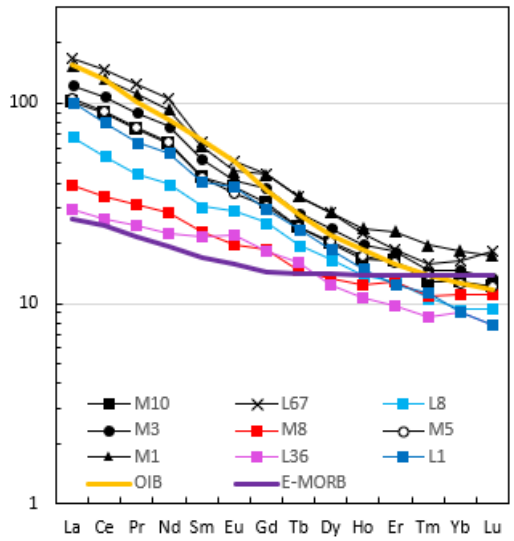

Fig. 6. Chondrite normalized diagrams. Normalizing values, OIB, and E-MORB after [39].

Multi-element diagrams normalized to the primitive mantle (Fig. 7), indicate enrichment in incompatible elements and depletion in compatible elements. The profiles exhibit a positive Ba anomaly relative to adjacent large-ion lithophile elements Rb and Th (Ba/Ba*=1.16–3.04). A trough in Th and U is observed in most samples. The tholeiitic dolerites exhibit different profiles, sample M8 displays a characteristic continental tholeiite (CT) profile with a significant negative Nb-Ta anomaly, whereas sample L36 shows a profile close to Enriched Mid-Ocean Ridge Basalts (E-MORB) and comparable to initial rifting tholeiites (IRT) [47].

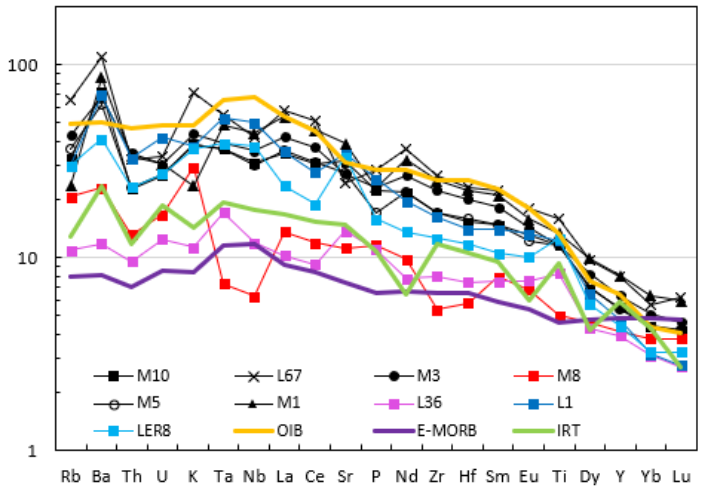

Fig. 7. Primitive mantle-normalized diagrams. Normalizing values, OIB, and E-MORB after [39]. IRT after [47] and [48] for Ta, Nd, Eu, Dy, and Lu.

Alkali dolerites show significant enrichment in high field strength elements such as Nb and Ta relative to light REE like La and large ion lithophile elements like K (Nb/Nb*=1.29–1.37, Ta/Ta*=1.33–1.44) resembling features observed in OIB patterns (Nb/Nb*=1.32, Ta/Ta*=1.30) after [39]. In contrast, transitional dolerites display marked depletion in Nb, (Nb/Nb* = 0.7–0.9) and relatively uncontrasted Ta levels compared to La and K, (Ta/Ta* = 0.9–1.1).

V. Discussion

5.1 Tectonic setting

The dolerite dykes are emplaced within the Precambrian basement and the Cretaceous intracontinental basins, indicating an intra-plate tectonic setting. In the K_2O-TiO_2-P_2O_5 diagram from [49] (not shown here), samples L36 and L40 plot within the field of oceanic tholeiites and IRT, while M8 falls within the continental tholeiite field. Similarly, in the TiO_2-Nb/3-Th diagram from [47] (not shown here), L36 plots within the plate-margin tholeiitic basalts and IRT field, whereas M8 is located within the within-plate tholeiitic basalts field.

Jean-Claude Doumnang Mbaigané, Léontine Tekoum, Pierre Rochette, and Jean-Paul Vicat, "The Dolerites of the Léré Region (Southwestern Chad, Africa): Petrography and Geochemical Characterisation," *International Journal of Multidisciplinary Research and Publications (IJMRAP)*, Volume 7, Issue 10, pp. 22-32, 2025.

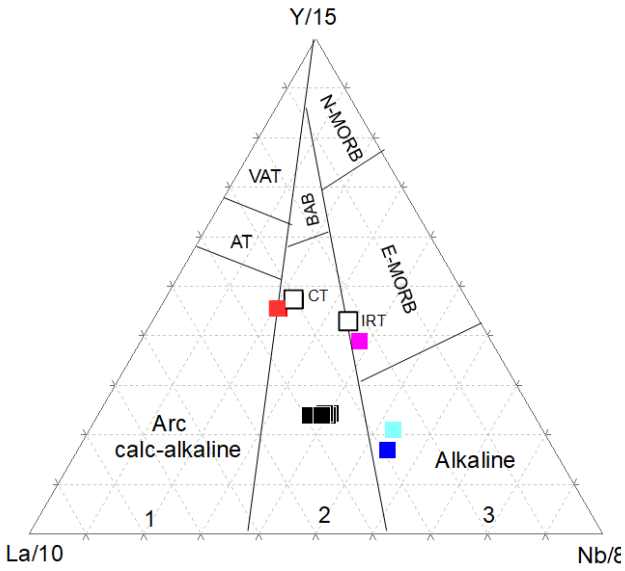

Fig. 8. Plot of Léré dolerites in the La/10-Y/15-Nb/8 diagram from [50]. 1: Orogenic domain. 2: Late to post-orogenic compressive to distensive domains. 3: Anorogenic distensive domains. VAT: Volcanic arc tholeiites. AT: Transitional arc volcanism. BAB: Back arc volcanism. CT: Continental tholeiites. IRT: Initial rifting tholeiites after [47]. Symbols as in Fig. 4

In the La/10-Y/15-Nb/8 diagram from [50] (Fig. 8), L8 and L1 are located within the alkaline anorogenic extensional domain, whereas M8 falls in the calc-alkaline orogenic domain near the CT of [47], reflecting its Nb depletion. L36 is positioned within the E-MORB domain, close to the IRT of [47]. The transitional dolerites plot in the intermediate domain between the orogenic and anorogenic fields, corresponding to the domain of CT.

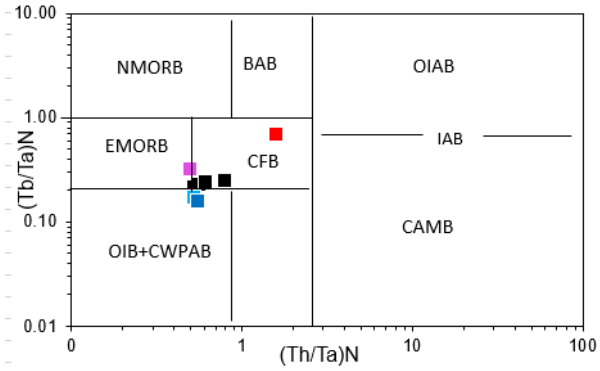

Fig. 9. Plot of Léré dolerites in the $(Tb/Ta)_N$ vs $(Th/Ta)_N$ diagram from [51]. The ratios are normalized to the estimated values for the Primordial Mantle after [52]. This diagram enables discrimination between: the N-MORB, the E-MORB, the continental within-plate alkaline and transitional basalts (CWPAB) + the OlB, the continental tholeiites (CT), part of the back-arc basins basalts (BAB), and the subduction-related lavas including those from Chilean type active margins (CAMB), Mariana-type intra-oceanic arcs (OIAB) and intermediate arcs (lAB). Symbols as in Fig. 4.

In the $(Tb/Ta)_N$ vs $(Th/Ta)_N$ diagram from [51] (Fig. 9), L8 and L1 plot in the continental within-plate alkaline basalts domain, in agreement with their alkaline nature. M8 is located in the continental tholeiites field. L36 plots at the boundary between continental tholeiites and E-MORB $(Th/Ta)_N$=0.5). The transitional dykes plot within the domain of continental tholeiites.

5.2 Crustal contamination

During their emplacement, the chemical composition of basic dykes is sometimes altered by the assimilation of crustal fragments, particularly in large-scale veins where the magma flow is turbulent rather than laminar [53].

Crustal contamination can be identified in the Rb/Y vs Nb/Y diagram from [54]. In this diagram (Fig. 10), the vertical trend of Léré dolerites is distinct from the Pan-African granitoid of the Léré region basement and the upper continental crust. This indicates the minimal importance of crustal contamination, except for M8.

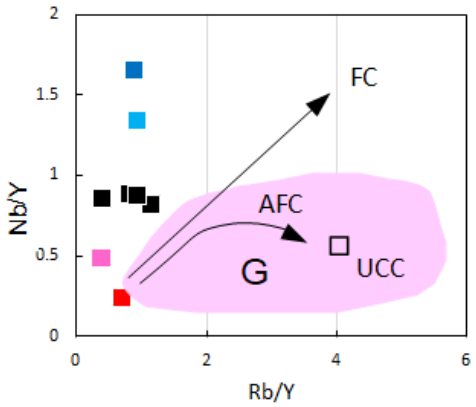

Fig. 10. Plot of Léré dolerites in the Nb/Y vs Rb/Y diagram from [54]. FC: Fractional crystallization. AFC: Assimilation fractional crystallization. G: Pan-African granitoids of the Léré region basement after [5, 55]. UCC: Upper continental crust after [59]. Symbols as in Fig. 4.

Incompatible trace element ratios such as Nb/U, Ba/Nb, and La/Nb are also commonly used to distinguish uncontaminated oceanic basaltic rocks (MORB/OIB) from basalts contaminated by continental crust [56, 57]. The Nb/U ratio in oceanic basalts is typically 47 ± 10 [58], 10 for the lower continental crust, and 4.44 for the Upper Continental Crust [59]. Apart from M8, the Nb/U ratios of the Léré dolerites (36.4–48.9) are similar to those of mantle-derived oceanic basalts, suggesting insignificant contamination effects for Nb/U. The low Nb/U ratio (12.9) of sample M8 indicates contamination by the crust. The Ba/Nb and La/Nb of the continental crust typically exhibits high ratios, which vary among authors [59–62], but are consistently higher than those of mantle-derived oceanic basalt, which range from Ba/Nb (4.3–17.8) and La/Nb (0.66–1.19) [56]. Except for M8, the observed Ba/Nb (8.7–25.7) and La/Nb (0.6–1.3) ratios of the Léré dolerites are similar to those of typical mantle-derived values. The high ratios in M8 (Ba/Nb=35.44, La/Nb=2.07) reflect crustal contamination. The previous diagram (Fig. 10), and these ratios indicate that the Léré dolerites underwent insignificant to low crustal contamination, except for M8, which shows some crustal contamination.

5.3 Fractional crystallization

The concentrations of Cr (20–295 ppm) in the dykes of Léré with low MgO values (4.01–6.79%) and Mg# (36–56) are lower

Jean-Claude Doumnang Mbaigané, Léontine Tekoum, Pierre Rochette, and Jean-Paul Vicat, "The Dolerites of the Léré Region (Southwestern Chad, Africa): Petrography and Geochemical Characterisation," *International Journal of Multidisciplinary Research and Publications (IJMRAP)*, Volume 7, Issue 10, pp. 22-32, 2025.

than those expected for primitive magma compositions with Cr >300–500 ppm, MgO (10–15%), and Mg# (68–72) [63, 64]. Therefore, the Léré dykes have undergone some crystallization processes before their emplacement at the surface.

The Léré dykes are all mafic (SiO2<52%); consequently, no chemical trend related to fractional crystallization processes can be observed in our data. However, the tholeiitic dolerites were not derived from transitional magmas by fractionation of clinopyroxene, due to their low concentrations of large-ion lithophile elements, Nb, Zr, and Y compared to those of transitional dolerites.

5.4 Depth of melt segregation and degree of partial melting

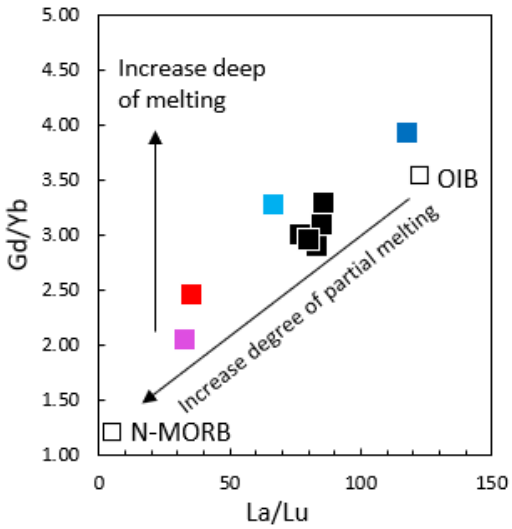

Fig. 11. Plot of Léré dolerites in the Gd/Yb vs La/Lu diagram from [65]. OIB and N-MORB after [39]. Symbols as in Fig. 4.

The compositional variations between alkali and tholeiitic dolerites may be due to different depths of magma segregation in the mantle source and variable degrees of partial melting. In the Gd/Yb vs La/Lu diagram from [65] (Fig. 11), the tholeiitic dolerites exhibit narrow ranges of La/Lu ratios and low values of the Gd/Yb ratio, whereas the alkali transitional dolerites show a range of La/Lu ratios extended and higher values of the Gd/Yb ratio. Therefore, the tholeiitic dolerites derive from a relatively shallow depth with a higher degree of partial melting than the alkali and transitional dolerites.

As shown in the $(Tb/Yb)_N$ vs. $(La/Yb)_N$ diagram after [66] (Fig. 12), the tholeiitic dolerite M8 originates from a mantle source within the stability field of the spinel zone at depths shallower than 80 km [67]. The tholeiitic dolerite (L36), the transitional dolerites, and the alkaline dolerite (L8) are derived from the garnet-spinel transition zone. The Dissing alkaline intrusion (L1) originates from the garnet stability field at depths greater than 80 km. The $(Tb/Yb)_N$ vs. Mg# diagram from [66] and the Dy/Yb vs. La/Yb diagram from [71] (not shown here) lead to the same conclusion.

The variable ratios of high to slightly incompatible elements such as Th/Tb (1.35–3.12), Ta/Tb (0.55–2.42), La/Sm (2.12–4.05) reflect varied degrees of melting [72] for the Léré dolerites.

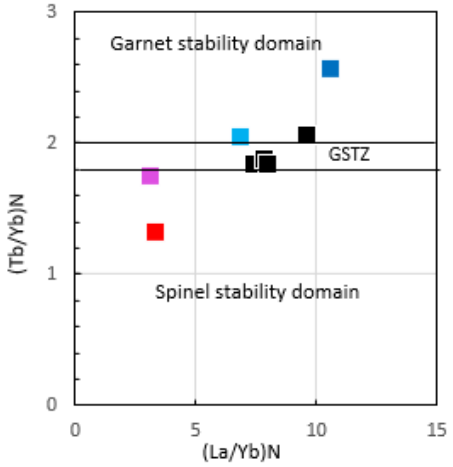

Fig. 12. (Tb/Yb)N versus (La/Yb)N plot of Léré dolerites, adapted from [66]. GSTZ: Garnet-Spinel Transition Zone. Normalizing values after [68]. Symbols as in Fig. 4

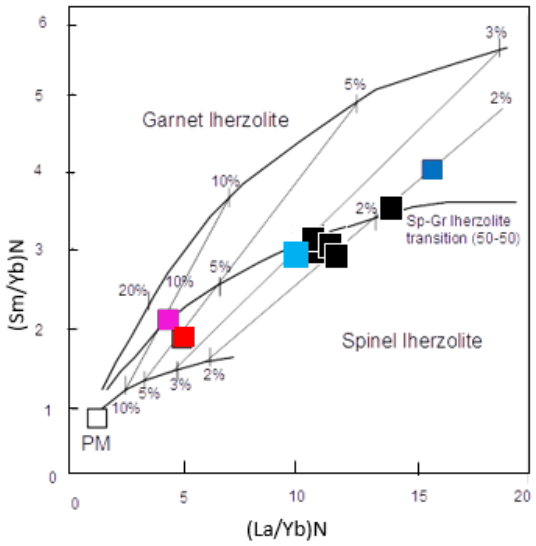

Fig. 13. Sm/Yb vs. La/Yb variation of Léré dolerite. Garnet and spinel lherzolites composition for modeling modified from [69, 70]. Symbols as in Fig. 4.

To evaluate the melting conditions, we applied a non-modal equilibrium melting model of garnet and spinel-bearing lherzolitic mantle sources using the primitive mantle of [39] as a starting point. In the Sm/Yb vs. La/Yb diagram (Fig. 13), the alkaline pluton from Dissing can be generated with 2% partial melting in the garnet lherzolite zone. The transitional dykes and the alkali dolerite L8 can be formed with approximately 2-3% partial melting near the spinel-garnet lherzolite transition zone of mantle sources. The tholeiitic dolerite L36 could have formed with about 10% partial melting near the spinel-garnet lherzolite transition zone, while M8 with about 5% partial melting in the spinel lherzolite zone.

5.5 Mantle sources

The sources of basic magmas can be identified using binary diagrams of incompatible elements, as their ratios reflect those of the mantle source and are not modified during differentiation. In the Th/Yb vs. Nb/Yb diagram from [73] (Fig. 14), three distinct sources are identified. The alkaline dolerite L1

Jean-Claude Doumnang Mbaigané, Léontine Tekoum, Pierre Rochette, and Jean-Paul Vicat, "The Dolerites of the Léré Region (Southwestern Chad, Africa): Petrography and Geochemical Characterisation," *International Journal of Multidisciplinary Research and Publications (IJMRAP)*, Volume 7, Issue 10, pp. 22-32, 2025.

originates from an OIB-type mantle source. Except for M8, the other dolerites come from an intermediate source between OIB and E-MORB, with alkaline dolerite L8 closer to OIB and tholeiitic dolerite L36 closer to E-MORB. The tholeiitic dolerite M8, originating from a source close to E-MORB, is affected by crustal contamination.

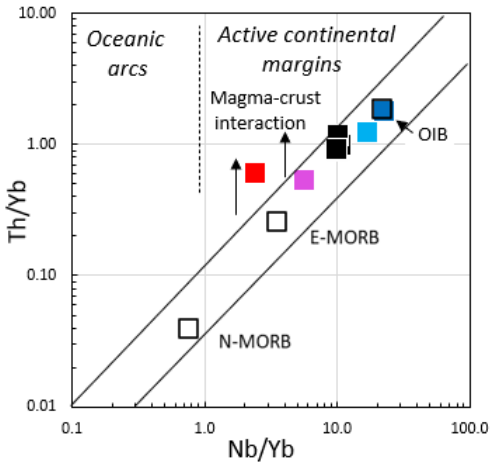

Fig. 14. Plot of Léré dolerites in the Th/Yb vs. Nb/Yb diagram from [73]. OIB, E-MORB, and N-MORB after [39]. Symbols as in Fig. 4.

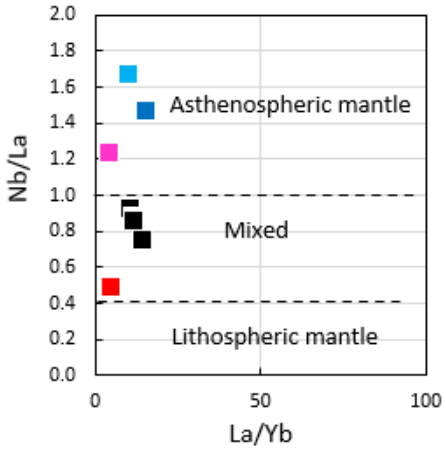

Fig. 15. Plot of Léré dolerites in the Nb/La vs. La/Yb diagram from [74]. Symbols as in Fig. 4.

The asthenospheric mantle is HFSE-enriched and HREE-depleted compared to the lithospheric mantle [74]. Therefore, high Nb/La ratios are characteristic of magmas derived from the asthenospheric mantle, whereas lower Nb/La ratios indicate derivation from the lithospheric mantle. In the diagram Nb/La vs. La/Yb from [74] (Fig. 15), the dolerite M8 plots close to a lithospheric source due to the Nb depletion of continental tholeiites contaminated by the continental crust. The transitional dolerites display low Nb/La ratios (<1), suggesting a mixed asthenospheric-lithospheric mantle source. The alkaline and IRT samples display high Nb/La ratios (>1), indicating an asthenospheric source nature. The La/Ba vs La/Nb diagram of [75, 76] (not shown here), which discriminates between asthenospheric and lithospheric magma origins, leads to the same conclusion.

5.6 Regional implications

The dolerites of the Léré region display diverse chemical compositions. The distinction between CT, IRT, transitional dolerites, and alkaline dolerites provides a framework for classifying dolerite analyses reported in the literature from the Mayo-Oulo and Léré basins [4, 7–10], attributed to tholeiitic or alkaline magmatism. According to these studies, CT and transitional dykes are restricted to the Proterozoic basement. Alkaline dolerites are relatively rare, with two dykes located at the eastern end of the Léré Basin and two other dykes crosscutting the Proterozoic basement. Dolerites with IRT signature are confined to the Cretaceous Mayo Oulo-Léré Basin. The formation of IRT, associated with lithospheric thinning during rifting, is consistent with the fact that the Mayo Oulo-Léré Basin constitutes the eastern termination of the Benue Trough, which is part of the West and Central African Rift System.

VI. Conclusion

This study reveals that the Léré dolerites exhibit diverse mineralogical and geochemical compositions. They consist of either clinopyroxene-orthopyroxene dolerites with an IRT composition or clinopyroxene-dolerites with CT, transitional, or alkaline compositions. The magmas that formed these dolerites originated from different depths and experienced varying degrees of partial melting. The IRT are restricted to the Cretaceous basin consistent with the basin's position within the West and Central African Rift System.

As the precise age of the Léré dolerites remains poorly constrained, this study emphasizes the need for radiometric datings. Such analyses would specify the exact emplacement age of the dykes associated with the Cretaceous basin and clarify the age of those intruding the Proterozoic basement, whose emplacement might be partly older.

Acknowledgement

The authors thank the Faculty of Exact and Applied Sciences of the University of N'Djaména (Chad) for facilitating the field and laboratory work. They also thank the French Ministry of Foreign Affairs for funding the chemical analyses.

References

[1] Guiraud R., Binks R. M., Fairhead J. D. and Wilson M. (1992). Chronology and geodynamic setting of Cretaceous-Cenozoic rifting in West and Central Africa. Tectonophysics, 213, 227–234. https://doi.org/10.1016/0040-1951(92)90260-D

[2] Guiraud R. and Maurin J.C. (1992). Early Cretaceous rifts of Western and Central Africa: an overview. Tectonophysics, 213, 153–168. https://doi.org/10.1016/0040-1951(92)90256-6

[3] Maurin J.C., and Guiraud, R. (1993). Basement control in the development of the early cretaceous West and central African Rift System. Tectonophysics, 228, 81–95. https://doi.org/10.1016/0040-1951(93)90215-6

[4] Ngounouno I., Guiraud R., Déruelle B. and Vicat J.P. (2001). Magmatismes tholéiitiques et alcalins des demi-grabens crétacés de Mayo-Oulo-Léré et de Babouri-Figuil (Nord du Cameroun-Sud du Tchad) en domaine d'extension continentale. Comptes Rendus de l' Academie des Sciences Serie IIa : Earth and Planetary Science, 333, 201–207. https://doi.org/10.1016/S1251-8050(01)01626-3

[5] Doumnang Mbaigané J.C. (2006). Géologie des formations néoprotérozoïques du Mayo Kebbi (Sud-Ouest du Tchad) : apport de la

pétrologie et de la géochimie : implications sur la géodynamique au Panafricain. Thèse, Université d'Orléans, France, 264 p.

[6] Fagny Mefire, A., Bardintzeff, J.M., Nkouandou, O.F., Lika Gbeleng, T.A., and Ngougoure Mouansie, S. (2019). Petrology and geochemistry of Hama Koussou dolerite dyke swarms (north Cameroon, central Africa). Journal of Geography, Environment and Earth Science International, 23(3), 1–19. https://doi.org/10.9734/jgeesi/2019/v23i330170

[7] Klamadji, M.N., Gountié Dedzo, M., Tchameni, R., and Dawaï, D. (2020). Petrography and geochemical characterization of dolerites from Figuil (northern Cameroon) and Léré (southwestern Chad). International Journal of Geosciences, 11(7), 459–482. https://doi.org/10.4236/ijg.2020.117023

[8] Klamadji, M.N., Gountié Dedzo, M., Tchameni, R., Hamadjoda, D.D., Biakan à Nyotok, P. C., and Onana, G. (2021. Fractional crystallization and crustal contamination of doleritic and trachytic dykes crosscutting the Cretaceous sedimentary basins from Figuil (North Cameroon) and Léré (South-Western Chad): geodynamic implications. Journal of Geoscience and Environment Protection, 9(12), 190–210

[9] Nkouandou O.F., Bardintzeff J.M., Fagny Mefire A., Koromi A.B., Mahamat O., and Ngougoure M.S. (2022). Geodynamic framework of the magmatic activity of Cretaceous Léré basin (Southwestern Chad, Central Africa). Journal of African Earth Sciences, 194(1), 104630. https://doi.org/10.1016/j.jafrearsci.2022.104630

[10] Gountié Dedzo M., Klamadji M.N., Zangmo Tefogoum G., Chako-Tchamabé B., Asaah A., and Tchameni R. (2023). Major, trace elements and Sr–Nd–Pb isotopes systematics of mafic dykes from the Figuil (northern Cameroon) and Léré (southwestern Chad) areas, Geological Journal, 2023, 1–27. https://doi.org/10.1002/gj.4892

[11] Wacrenier P. (1962). Carte géologique de reconnaissance des Etats d'Afrique Equatoriale, feuille NC-33 SO E-53 SE O-54 (Moundou) au 500 000ème. IRGM, Brazzaville.

[12] Wolff J.P. (1964). Carte géologique de République du Tchad au 1/1 500 000. B.R.G.M, Paris.

[13] Schneider, J.L. (1989). Géologie et hydrogéologie de la République du Tchad. Thèse, Université d'Avignon, France, 547 p.

[14] Kasser, M.Y. (1995). Evolution précambrienne de la région du Mayo Kebbi (Tchad). Un segment de la chaîne panafricaine. Thèse, Muséum National Histoire Naturelle Paris, France, 217 p.

[15] Penaye J., Kröner A., Toteu S. F., Van Schmus W. R., and Doumnang J.C. (2006). Evolution of the Mayo Kebbi region as revealed by zircon dating: An early (ca. 740 Ma) Pan-African magmatic arc in southwestern Chad. Journal of African Earth Sciences, 44, 530–542. https://doi.org/10.1016/j.jafrearsci.2005.11.018

[16] Pouclet A., Vidal, M. Doumnang Mbaigané J.C., Vicat J.P., and Tchameni, R. (2006). Neoproterozoic crustal evolution in Southern Chad: Pan-African ocean basin closing, arc accretion and late- to post-orogenic granitic intrusion. Journal of African Earth Sciences, 44(4-5), 543–560.

[17] Mbaguedje, D. (2015). Métallogénie de l'or et de l'uranium dans le cadre de la croissance et de la différenciation de la croûte au Néoprotérozoïque : Exemple du massif du Mayo-Kebbi (Tchad) dans la Ceinture Orogénique d'Afrique Centrale. Thèse, Université de Lorraine, France, 269 p.

[18] Bessoles B. and Trompette R. (1980). Géologie de l'Afrique : La chaine panafricaine, zone mobile d'Afrique Centrale (partie Sud) et zone soudanaise. Mémoire BRGM, 92, 317 p.

[19] Castaing C., Feybesse J. L., Thyéblemont D., Triboulet C., and Chevremont P. (1994). Paleographical reconstruction of the Pan-African / Brasiliano orogen: closure of an oceanic domain or intracontinental convergence between major blocks. Precambrian Research, 69, 327–344.

[20] Toteu S.F., Penaye J., and Poudjom Djomani Y.H. (2004). Geodynamic evolution of the Pan-African belt in Central Africa with special reference to Cameroon. Canadian Journal of Earth Sciences, 41, 73–85. https://doi.org/10.1139/e03-079

[21] Toteu S.F., Van Schmus R.W., Penaye J., and Michard A. (2001). New U–Pb and Sm–Nd data from north-central Cameroon and its bearing on the pre-Pan-African history of central Africa. Precambrian Research, 108, 45–73. https://doi.org/10.1016/S0301-9268(00)00149-2

[22] Bessong M., Hell J.V., Elias S., Susanne F.B., Eyong J.T., Ngos SIII., Nolla J.D., Mbesse C.O., Thierry A., Mfoumbeng M.P., Dissombo Edimo A.N., Ntsama Atangana J., Mouloud B., and Ndjeng E. (2018). Hydrocarbon potential, palynology and palynofacies of four sedimentary basins in the Benue Trough, northern Cameroon. Journal of African Earth Sciences, 139, 73–95. https://doi.org/10.1016/j.jafrearsci.2017.11.012

[23] Maurin J.C., and Guiraud, R. (1990). Relationships between tectonics and sedimentation in the Barrémo-Aptian intracontinental basins of Northern Cameroon. Journal of African Earth Sciences, 10, (1-2). 331–340. https://doi.org/10.1016/0899-5362(90)90064-L

[24] Fosso Menkem E., Ngounou Ngatcha B., Ngia N. R., Fuanya C., and Ekodeck G.E. (2024).Tectonic and sedimentary evolution of the Northern Cameroon Cretaceous rift basins: A study of the Babouri-Figuil and Mayo Oulo-Lere basins. Geosystems and Geoenvironment, 3, 100291. https://doi.org/10.1016/j.geogeo.2024.100291

[25] Tchouatcha M.S., Azinwi Tamfuh P., Sobdjou Kemteu C., Mbesse C.O., and Ngnotue T. (2021a). Provenance, palaeoweathering and depositional environment of the cretaceous deposits from the Babouri-Figuil and Mayo Oulo-Lere basins (North-Cameroon) during the Southern Atlantic opening: geochemical constraints. Journal of African Earth Sciences, 174, 104052. https://doi.org/10.1016/j.jafrearsci.2020.104052.

[26] Tchouatcha M.S., Sobdjou Kemteu C., Mbesse C.O., Ouandji Sime L.L., Miyemeck Ngonlep V.T., and Tchounang Kouonang S. (2021b). Mechanisms of sedimentation in lacustrine environment of Babouri-Figuil and Mayo Oulo-Lere basins deposits (North Cameroon) during the Southern Atlantic opening: sedimentary structures and geochemistry constraints. Arabian Journal of Geosciences, 14(6), 450. https://doi.org/10.1007/s12517-021-06763-7

[27] Brunet M., Dejax J., Brillanceau A., Downs W., Duperon Laudoueneix M., Eisenman V., Flanagan K., Flynn E., Heintz E., Hell J., Jacob L., Jehene Y., Ndjeng E., Mouchelin G., and Pibleam D. (1988). Mise en évidence d'une sédimentation précoce d'âge barrémien dans le fossé de la Bénoué en Afrique Occidentale (bassin du MayoOulo-Léré) en relation avec l'ouverture de l'Atlantique Sud. Comptes Rendus de l'Académie des Sciences, Paris 306(II), 1125–1130.

[28] Ngo Elogan Ntem, J., Ngounfack Tiokeng V, Toyama R, Berinyuy Konglim Y., Takoi J.F., Togoum N., Ngnotue T., and Tchouatcha M. S. (2024). Geochemical constrains for unravelling the condition of sedimentation, provenance, paleoclimate variation, and metallogenic implication of the cretaceous deposits of Mayo Oulo Basin (North Cameroun, Africa). Solid Earth Sciences, 9, 100188. https://doi.org/10.1016/j.sesci.2024.100188

[29] Ndjeng E. (1992). Etude de la sédimentologie et du modèle d'évolution géodynamique de deux bassins du Crétacé inférieur du Nord Cameroun : Babouri-Figuil et Mayo Oulo- Léré. Thèse, Université de Yaoundé, Cameroun, 311 p.

[30] Benkhelil J. (1986). Structure et évolution géodynamique du bassin intracontinental de la Bénoué (Nigeria). Thèse Sciences, Université de Nice, France, 231 p.

[31] Guiraud R. Bellion Y. Benkhelil J. and Moreau C. (1987) Post-Hercynian Tectonics in Northern and Western Africa. Geology Journal, 22, 433–466. https://doi.org/10.1002/gj.3350220628,

[32] Guiraud R. and Bellion Y. (1995). Late Carboniferous to Recent Geodynamic Evolution of the West Gondwanian, Cratonic, Tethyan Margins. In: Nairn, A., Dercourt, J. and Vrielynck, B., (Eds), The Ocean Basins and Margins, 8, The Tethys Ocean, 101–124. https://doi.org/10.1007/978-1-4899-1558-0_3

[33] Wilson M., Guiraud R., Moreau C., and Bellion Y.J.C. (1998). Late Permian to Recent Magmatic Activity on the African-Arabian Margin of Tethys. In: Macgregor, D.S., Moody, R.T.J. and Clark-Lowes, D.D. (Eds.), Petroleum Geology of North Africa, Geological Society. London Special Publications, 132, 231–263. https://doi.org/10.1144/GSL.SP.1998.132.01.14

[34] Genik G.J. (1992). Regional framework, structural and petroleum aspects of rift basins in Niger, Chad and the Central African Republic (C.A.R.). Tectonophysics, 213, 169–185. https://doi.org/10.1016/B978-0-444-89912-5.50036-3

[35] Béa A., Cochemé J.J., Trompette R., Affaton P., Soba D., and Sougy J. (1990). Grabens d'âge paléozoïque inférieur et volcanisme tholéiitique associé dans la région de Garoua au Nord-Cameroun. Journal of African Earth Sciences, 10(4), 657–667. https://doi.org/10.1016/0899-5362(90)90032-A

[36] Shellnutt J.G., Lee T.Y., Yang C.C., Hu S.T., Wu J.C., Wang K.L, and Lo C.H. (2015). Late Permian mafic rocks identified within the Doba basin of southern Chad and their relationship to the boundary of the Saharan Metacraton. Geological Magazine, 1, 1-12.

[37] Nkouandou O.F., Bardintzeff J.M., Mahamat O., Fagny Mefire A., and Ganwa A.A. (2017). The dolerite dyke swarm of Mongo, Guéra Massif (Chad, Central Africa): Geological setting, petrography and geochemistry. Open Geosciences, 9, 138–150. https://doi.org/10.1515/geo-2017-0012

[38] Carignan J., Hild P., Mevelle G., Morel J., and Yeghicheyan D. (2001). Routine analyses of 551 trace elements in geological samples using flow injection and low-pressure on-line liquid 552 chromatography coupled to ICP-MS: a study of reference materials BR, DR-N, UB-N, AN-G553, and GH. Geostandards and Geoanalytical Research, 25, 187–198.
[39] Sun S.,and McDonough W. (1989). Chemical and isotopic systematics of ocean basalts: implications for mantle composition and processes. Geological Society of London Special Publication, 42, 313–345. 10.1144/GSL.SP.1989.042.01.19
[40] Hughes C.J. (1973). Spilites, keratophyres and the igneous spectrum. Geological Magazine, 109, 513–527
[41] Bau M. (1996). Controls on the fractionation of isovalent trace elements in magmatic and aqueous systems: evidence from Y/ho, Zr/Hf, and lanthanide tetrad effect. Contribution to Mineralogy and Petrology, 123, 323–33. https:// doi. org/ 10. 1007/ s0041 00050 159
[42] Le Bas M.J., Le Maitre R.W., Streckeisen A., and Zanettin B. (1986). A chemical classification of volcanic rocks based on the total alkali–silica diagram. Journal of Petrology, 27, 745–750.
[43] Irvine T.N., and Baragar W.R.A. (1971). A guide to chemical classification of the common volcanic rocks. Canadian Journal of Earth Sciences, 8, 523–548. https://doi.org/10.1139/e71-055
[44] Winchester J.A., and Floyd P.A. (1977). Geochemical magma type discrimination: application to altered and metamorphosed basic igneous rocks. Earth and Planetary Science Letters, 28(3), 459–469. https://doi.org/10.1016/0009-2541(78)90050-5
[45] Pearce J.A. and Cann J.R. (1973). Tectonic Setting of Basic Volcanic Rocks Determined Using Trace Element Analyses. Earth and Planetary Science Letters, 19, 290-300. https://doi.org/10.1016/0012-821X(73)90129-5
[46] Miyashiro, A. (1975). Classification, Characteristics, and Origin of Ophiolites. Journal of Geology, 83 (2), 249–281.
[47] Holm P.E. (1985). The geochemical fingerprints of different tectonomagmatic environments using hygromagmatophile element abundances of tholeiitic basalts and basaltic andesites. Chemical Geology, 51, 303–323. https://doi.org/10.1016/0009-2541(85)90139-1
[48] Álvaro J.J., Pouclet A., Ezzouhairi H., Abderrahmane Soulaimani A., Bouougri E.H, Imaze A.G., and Fekkak A. (2014). Early Neoproterozoic rift-related magmatism in the Anti-Atlas margin of the West African craton, Morocco. Precambrian Res.
[49] Pearce T.H., Gorman B.E., and Birkett T.C. (1975). The TiO2–K2O–P2O5 diagram: a method of discriminating between oceanic and non-oceanic basalts. Earth and Planetary Science Letters, 24, 419–426. https://doi.org/10.1016/0012-821X(75)90149-1
[50] Cabanis B., and Lécolle, M. (1989). Le diagramme La/10-Y/15-Nb/8: un outil pour la discrimination des séries volcaniques et la mise en évidence des processus de mélange et/ou de contamination crustale. Comptes Rendus de l'Académie des Sciences, Paris, 309, 2023–2029.
[51] Thiéblemont D., Chevremont P., Castaing C., and Feybesse J.L. (1994). La discrimination géotectonique des roches magmatiques basiques par les éléments traces : reévaluation d'après une base de données et application à la chaîne panafricaine du Togo. Geodinamica Acta, 7(3), 139–157. https://doi.org/10.1080/09853111.1994.11105264
[52] Hofmann A.W. (1988). Chemical differentiation of the Earth: the relationship between mantle, continental crust, and oceanic crust. Earth and Planetary Science Letters, 90, 297–314. https://doi.org/10.1016/0012-821X(88)90132-X
[53] Campbell I.H. (1985). The difference between oceanic and continental tholeiites: a fluid dynamic explanation. Contrib. Mineral. Petrol, 91, 37–43. https://doi.org/10.1007/BF00429425
[54] Cox K. G., and Hawkesworth C. J. (1985). Geochemical stratigraphy of the Deccan Traps at Mahabaleshwar, Western Ghats, India, with implications for open system magmatic processes. Journal of Petrology, 26, 355–377. https://doi.org/10.1093/petrology/26.2.355
[55] Isseini M., André-Mayer A. S., Vanderhaeghe O., Barbey P., and Deloule E. (2012). A-type granites from the Pan-African Orogenic Belt in southwestern Chad constrained using geochemistry, Sr-Nd isotopes and U-Pb geochronology. Lithos, 153, 39–52.
[56] Weaver B.L. (1991). The origin of ocean island basalt end-member compositions: trace element and isotopic constraints. Earth and Planetary Science Letters, 104(2-4), 381–397.
[57] Hess P. C. (1992). Phase Equilibria Constraints on the Origin of Ocean Floor Basalts. In. in: Phipps Morgan J., Blackman D.K., and Sinton J.M. (Eds.), Mantle Flow and Melt Generation at Mid-Ocean Ridges, 67–102.
[58] Hofmann A. W. (2003). Sampling mantle heterogeneity through oceanic basalts: Isotopes and trace elements. Treatise on Geochemistry, 2, 568.
[59] Rudnick R.L. and Gao S. (2004). Composition of the continental crust. In: Holland, H.D., and Turekian, K.K. (Eds.), Treatise on Geochemistry, 3, 1–64.
[60] Weaver B.L., and Tarney J. (1984). Empirical approach to estimating the composition of continental crust. Nature, 310, 575–577.
[61] Taylor S.R., and McLennan S.M. (1985). The Continental Crust: its Composition and Evolution. Blackwell scientific publications, 312 p.
[62] Rudnick R.L. and Fountain D.M. (1995). Nature and composition of the continental crust: a lower crustal perspective. Reviews of Geophysics, 33, 267–309. https://doi.org/10.1029/95RG01302
[63] Frey F.A., Green D.H., and Roy S.D. (1978). Integrated models of basalt petrogenesis: a study of quartz tholeiites to olivine melilitites from South Eastern Australia utilizing geochemical and experimental petrological data. Journal of Petrology, 19, 463–513.
[64] Jung S., and Masberg P. (1998). Major- and trace-element systematics and isotope geochemistry of Cenozoic mafic volcanic rocks from the Vogelsberg (Central Germany): Constraints on the origin of continental alkaline and tholeiitic basalts and their mantle sources. Journal of Volcanology and Geothermal Research, 86, 151–177. https://doi.org/10.1016/S0377-0273(98)00087-0
[65] Girum B., Takele Chekol T., and Meshesha D. (2023). Petrological and geochemical characteristics of flood and shield basalts from Kesem-Megezez section, northwestern Ethiopian Plateau: Implication for their mantle source variations. Heliyon, 9, e17256. https://doi.org/10.1016/j.heliyon.2023.e17256
[66] Wang K., Plank T., Walker J.D., and Smith E.I. (2002). A mantle melting profile across the Basin and Range, SW USA. Journal of Geophysical Research, 107(b1). https://doi.org/ 10.1029/2001JB000209
[67] Takahashi E., and Kushiro I. (1983). Melting of a dry peridotite at high pressures and basalt magma genesis. American Mineralogist, 68, 859–879.
[68] McDonough, W.F., and Sun, S.S. (1995). The composition of the Earth. Chemical Geology, 12, 223–253. https://doi.org/10.1016/0009-2541(94)00140-4
[69] Aldanmaz E., Pearce J.A., Thirlwall M.F., and Mitchell J.G. (2000). Petrogenetic evolution of late Cenozoic, post-collision volcanism in western Anatolia. Turkey. Journal of Volcanology and Geothermal Research, 102(1-2), 67–95. https:// doi. org/ 10. 1016/ S0377- 0273(00) 00182-7.
[70] Tamirat T., Chekol T., and Meshesha D. (2021). Petrology and geochemistry of basaltic rocks from north western Ethiopian plateau continental flood Basalt Journal of African Earth Sciences, 182, 104282. https://doi.org/10.1016/j.jafrearsci.2021.104282
[71] Jung C., Jung S., Hoffer E., and Berndt J. (2006). Petrogenesis of tertiary mafic alkaline magmas in the Hocheifel, Germany. Journal of Petrolog, 4, 1637–1671. https://doi.org/10.1093/petrology/egl023
[72] Treuil M., and Joron L. (1976). Etude géochimique des éléments en trace dans le magmatisme de l'Afar. Implication pétrogénétique et comparaison avec le magmatisme de l'Islande et de la dorsale medio atlantique. Report n° 16. Procedings of an international symposium on the Afar region and related rift problems. Bad Bergrabern F.R. Germany.
[73] Pearce J.A. (2008). Geochemical fingerprinting of oceanic basalts with applications to ophiolite classification and the search for Archean oceanic crust. Lithos, 100, 14–48. https://doi.org/10.1016/j.lithos.2007.06.016
[74] Smith E.I., Sanchez A., Walker J.D., and Wang K. (1999). Geochemistry of mafic magmas in the Hurricane Volcanic Field, Utah: implications for small- and large-scale chemical variability of the lithospheric mantle. The Journal of Geology, 107(4), 433–448. http://dx.doi.org/10.1086/314355
[75] Fitton J. G., James D. and Leeman W. P. 1991. Basic magmatism associated with the late Cenozoic extension in the western United States: compositional variations in space and time. Journal of Geophysical Research, 96, 13693–13711. https://doi.org/10.1029/91JB00372
[76] Saunders A.D., Storey M., Kent R.W., and Norry M.J. (1992). Consequences of plume–lithosphere interactions. In Magmatism and the Causes of Continental Break-up, B.C. Storey, T. Alabaster, and R.J. Pankhurst Eds, Geological Society, London, Special Publication, 68, 41–60.